The Journal of Neuroscience, September 1, 2001, 21(17):6905–6916

Neural Coding Mechanisms Underlying Perceived Roughness of Finely Textured Surfaces

Takashi Yoshioka, Barbara Gibb, Andrew K. Dorsch, Steven S. Hsiao, and Kenneth O. Johnson

Zanvyl Krieger Mind/Brain Institute, Departments of Neuroscience and Biomedical Engineering, Johns Hopkins University, Baltimore, Maryland 21218

Combined psychophysical and neurophysiological studies have shown that the perceived roughness of surfaces with element spacings of >1 mm is based on spatial variation in the firing rates of slowly adapting type 1 (SA1) afferents (mean absolute difference in firing rates between SA1 afferents with receptive fields separated by ~2 mm). The question addressed here is whether this mechanism accounts for the perceived roughness of surfaces with element spacings of <1 mm. Twenty triangular and trapezoidal gratings plus a smooth surface were used as stimulus patterns [spatial periods, 0.1–2.0 mm; groove widths (GWs), 0.1–2.0 mm; and ridge widths (RWs), 0–1.0 mm]. In the human psychophysical studies, we found that the following equation described the mean roughness magnitude estimates of the subjects accurately (0.99 correlation): $0.2 + 1.6GW - 0.5RW - 0.25GW^2$. In the neurophysiological studies, these surfaces were scanned across the receptive fields of SA1, rapidly adapting, and Pacinian (PC) afferents, innervating the glabrous skin of anesthetized macaque monkeys. SA1 spatial variation was highly correlated (0.97) with human roughness judgments. There was no consistent relationship between PC responses and roughness judgments; PC afferents responded strongly and almost equally to all of the patterns. Spatial variation in SA1 firing rates is the only neural code that accounts for the perceived roughness of surfaces with finely and coarsely spaced elements. When surface elements are widely spaced, the spatial variation in firing rates is determined primarily by the surface pattern; when the elements are finely spaced, the variation in firing rates between SA1 afferents is determined by stochastic variation in spike rates.

Key words: roughness; tactile; somatosensory; grating; fine texture; peripheral nerve; SA1; RA; PC; psychophysical roughness magnitude; macaque; mechanoreceptor

This is the fourth in a series of combined psychophysical and neurophysiological studies of the neural coding mechanisms underlying roughness perception (Connor et al., 1990; Connor and Johnson, 1992; Blake et al., 1997). Each of the three previous studies used identical textured surfaces in neurophysiological and psychophysical experiments. All hypotheses concerning the neural basis for roughness perception of which we are aware were tested; hypothetical neural coding measures were rejected only when there was no consistent relationship with the human subjects' roughness judgments. All neural codes based on mean impulse rates failed this consistency test in the first and second studies. All neural codes based on Pacinian (PC) and cutaneous rapidly adapting (RA) afferent responses were rejected in the first and third studies. Temporal codes were rejected in the second study. The single neural code that emerged as a viable basis for roughness perception was spatial variation in slowly adapting type 1 (SA1) firing rates, which was computed as the mean absolute difference in firing rates between SA1 afferents with receptive field centers separated by ~2 mm. The correlation between this neural measure and the subjects' roughness judgments was 0.97 or higher in all studies. Connor et al. (1990) observed that this measure of the SA1 neural activity is computed by any central neuron with excitatory and inhibitory subfields separated by ~2 mm, and DiCarlo and Johnson (2000) have demonstrated the existence of such neurons in primary somatosensory (SI) cortex. This leads to the hypothesis that roughness perception depends on the mean impulse rate of a population of central neurons that compute the spatial variation in SA1 impulse rates.

A concern is that these conclusions are based on stimuli with element spacings of 1 mm or greater. The question addressed here is whether spatial variation in the firing rates of SA1 afferents can account for roughness perception when the element spacing is finer than the SA1 innervation density (~1 afferent/mm^2) (Johansson and Vallbo, 1979; Darian-Smith and Kenins, 1980). There are two specific concerns. First, SA1 afferents might respond to finely textured surfaces too weakly to account for roughness perception. Second, and more compelling, even if the firing rates are substantial, how can spatial variation in those firing rates account for roughness perception when the surface feature density is higher than the SA1 innervation density and finer than the receptive field diameter? Because of concerns like these, Hollins and Risner (2000) have advanced a theory of roughness perception that is based on the conjecture of Katz (1925) that spatial mechanisms account for the perceived roughness of coarse surfaces and vibratory mechanisms (presumably PC afferents) account for the perceived roughness of fine surfaces. In the present study we ask the following two questions: (1) whether any aspect of the PC response can account for the perceived roughness of finely textured surfaces and (2) whether spatial variation in SA1 firing rates can do so.

MATERIALS AND METHODS

Stimulus surfaces. Twenty triangular and trapezoidal grating patterns and a smooth pattern were used in the psychophysical and neurophysiological

Received Jan. 24, 2001; revised June 13, 2001; accepted June 13, 2001.

This work was supported by National Institutes of Health Grants NS 18787 and NS 34086. We thank Justin Killebrew, John Lane, and Steve Patterson for their technical support.

Correspondence should be addressed to Dr. Takashi Yoshioka, Zanvyl Krieger Mind/Brain Institute, Johns Hopkins University, 338 Krieger Hall, 3400 North Charles Street, Baltimore, MD 21218. E-mail: takashi@jhu.edu.

 0270-6474/01/216905-12$15.00/0

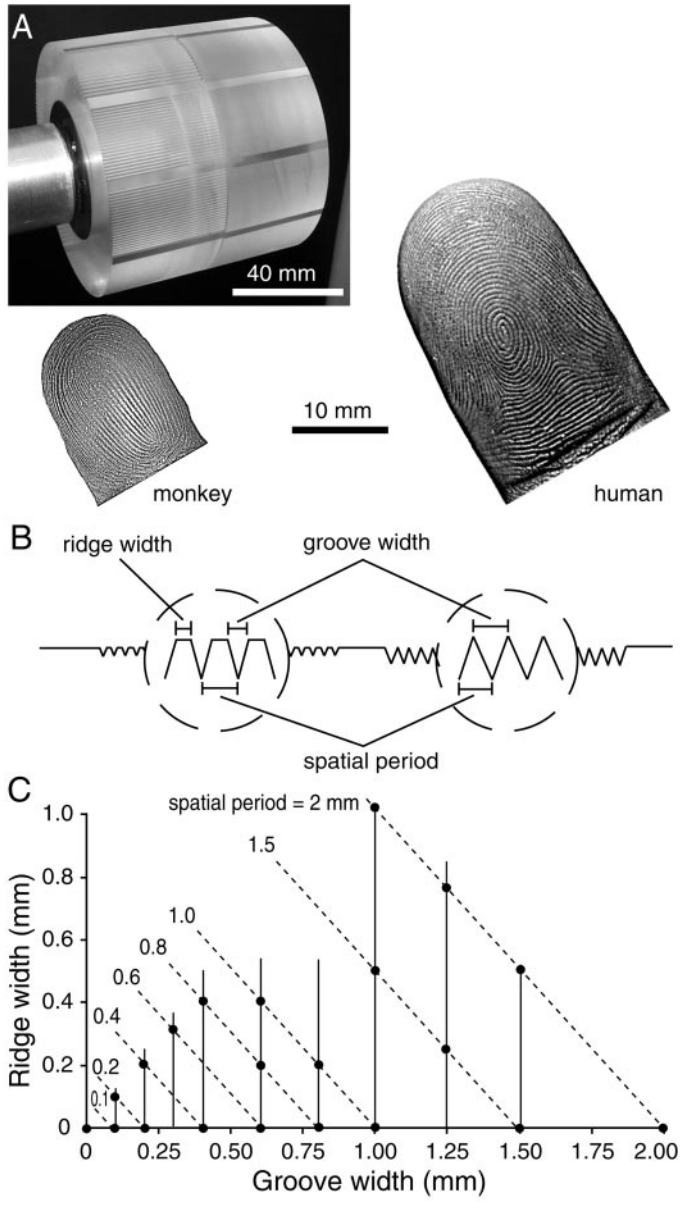

Figure 1. Stimulus patterns. *A*, Drum with grating stimuli machined into its surface and photographs of typical monkey and human distal fingerpads. Note the differences in skin ridge patterns between humans and monkeys. *B*, Cross-sectional view of a trapezoidal (*left*) and triangular (*right*) grating. *C*, Groove and ridge widths of all 21 gratings. The surfaces were designed so that almost all spatial periods (except 0.1 mm) comprised two or more combinations of GW and RW (*dashed lines*), almost all GWs (except 0.3 mm) were paired with two or more RWs (*solid lines*), and most RWs were paired with two or more GWs. The surface at 0 mm GW and RW is the smooth surface.

experiments. The gratings were machined into the surface of an acrylic plastic drum with a computer-controlled milling machine. The drum was 76 mm wide and 280 mm in circumference and contained 21 surfaces (20 gratings and a smooth surface). Each surface occupied 25.4 mm of drum circumference (1/11th of the drum circumference comprising a 23 mm grating and a flat ridge 2.4 mm wide) and either the entire drum width (smooth surface) or half (38 mm) of the width (Fig. 1*A*). The grating grooves and ridges were parallel with the drum axis; the sides of the ridges rose steeply (at 67.5° with respect to the horizontal, scanning plane; i.e., the grooves were machined with a 45° cutting tool). Because the sides of the ridges rose so steeply and the grooves were so deep relative to the groove width (groove depth = 1.2 × groove width), the skin touched only the ridges.

The surface design is illustrated in Figure 1, *B* and *C*. Because the grating spatial period equals the ridge width (RW) plus the groove width (GW), it is not possible to control all three independently, but the combinations include two or more gratings for most GWs, most RWs, and most spatial periods. If the psychophysical (or neural) response is determined solely or mostly by any one of these three parameters, then the response should be invariant between surfaces in which this parameter is constant. Because the emphasis is on surfaces with fine structure, 14 surface patterns have a spatial period of 1.0 mm or less.

Psychophysical methods. The drum with the stimulus surfaces was mounted on a servomotor apparatus and hidden from the subject's view by a screen. Subjects inserted their right hand through the screen and rested the wrist on a plate so that the distal pad of the index finger lay over an aperture 25 mm long (along the finger axis) and 34 mm wide. The drum was positioned on each trial so that one surface pattern, selected at random, was positioned beneath the subject's finger. Between trials, subjects raised their finger to allow positioning of the next stimulus surface. Subjects explored the surface by moving the right index finger repeatedly in a distal-to-proximal direction across the grooves and ridges. Because the finger was angled down slightly and because distal-to-proximal motion produces flexion, the skin ridges were parallel with the grating ridges through most or all of the movement (Fig. 1*A*). The force between the finger and the stimulus surface was maintained by a servomotor at 1.0 N, which is at the center of the force range used by humans when they actively scan surfaces in a roughness magnitude estimation experiment (Lederman, 1974).

Roughness was not defined for the subjects; instead, they were told to use their own concept of roughness from daily experience and to report how rough each surface felt with a number proportional to the strength of their perception of roughness. The surfaces were then presented in five randomized blocks, which yielded five responses per surface. Because roughness judgments are subjective, no feedback was given. The psychophysical data from each subject were normalized by dividing each numerical response by the mean of all of the subject's responses. The normalized values were averaged within subjects to produce a value for each surface and then across subjects to produce a grand mean for each of the 21 surfaces.

Neurophysiological methods. Four anesthetized macaque monkeys (*Macaca mulatta*) weighing between 3 and 8 kg were used for the experiment. The animals were sedated with ketamine (20 mg/kg, i.m.), placed on a vibration isolation table (Kinetic Systems, Inc., Roslindale, MA), and then anesthetized with Nembutal (sodium pentobarbital; 25 mg/kg, i.v.); additional doses of Nembutal were given to keep the animals areflexic. The experimental protocol complied with the guidelines of the Johns Hopkins University Animal Care and Use Committee and the *National Institutes of Health Guide for the Care and Use of Laboratory Animals*. Single mechanoreceptive fibers were dissected from the median or ulnar nerves with methods described previously (Mountcastle et al., 1972). Primary afferent fibers were classified as SA1, RA, or PC fibers on the basis of their responses to indentation and vibration with a point probe (Talbot et al., 1968). Neurons were excluded only if their receptive fields were not on one of the pads of the hand (digital pads, palmar pads, thenar eminence, and hypothenar eminence).

After the receptive field was mapped, the drum was placed on the receptive field and rotated to produce lateral motion between the stimulus surface and the skin (Johnson and Phillips, 1988). The drum was aligned so that the grating ridges were oriented parallel to the long axis of the finger. Because the skin ridges in the monkey finger run parallel to the finger axis (Fig. 1), this resulted in medial-to-lateral scanning across the monkey's fingerpad. The contact force and scanning velocity were 0.3 N and 20 mm/sec, respectively. Because of the differences in monkey and human finger size, 0.3 N produces approximately the same contact pressure as in the psychophysical experiments (Vega-Bermudez and Johnson, 1999). The velocity is not critical because roughness perception is unaffected over a wide velocity range (at least 10–70 mm/sec) (Lederman, 1974, 1983). After each surface scan (drum rotation), the drum was stepped 0.2 mm along the drum axis to avoid stimulating the receptive field with exactly the same surface segments (to average out the effects of any minute surface imperfections). At least 10 scans were made for each surface for each afferent fiber.

Analyses. All of the gratings were used in both the psychophysical and neurophysiological studies, but data from some triangular gratings (RW = 0) were excluded from the neurophysiological analyses because of a machining error. To get sharp ridges, it is necessary to set the cutting blade so that the ridges are slightly below the top of the surface being

milled. These depths have no effect on the psychophysical results; subjects place their fingers down until they touch the surfaces whatever the height. However, a difference in height between the smooth, unmachined surfaces of the drum, which separate the gratings (Fig. 1), and the peaks of the ridges produces a sudden change in skin indentation when the drum rotates over the skin surface. The drum is programmed to apply constant force, but it is also damped to keep it from bouncing when the surface elevation rises suddenly as it does, for example, when the surface elements are widely spaced (Johnson and Phillips, 1988). Conversely, when the surface drops away suddenly, it takes some time for the contact force to be reestablished. It would have been better to have left a small flat ridge on even the sharpest gratings to avoid any transition in surface elevation. The neural data from the finest triangular grating (GW = 0.1 mm) were retained because the ridge peaks were only 12 μm below the drum surface; neural data from the remaining seven triangular gratings were eliminated because the triangular peaks were 100–200 μm below the unmachined surfaces.

Action potential times and drum position signals, which were recorded with 0.1 msec precision, were used to construct two-dimensional spatial event plots in which each action potential was assigned x and y coordinates corresponding to the position of the stimulus pattern when the action potential occurred (Johnson and Phillips, 1988). All analyses were confined to a region 7 mm long beginning 8 mm after the start of each stimulus pattern.

Cycle histograms were constructed by assigning action potentials to bins according to their location within the stimulus grating cycle. A Fourier transform of this histogram was then used to analyze the relationship between the neural discharge and the stimulus. Because the gratings move continuously over receptive fields that are at least as large as the coarsest grating period and because there is an unknown delay between action potential initiation and its arrival at the recording site, the starting phase in the period histogram is arbitrary. For this reason, all histograms were rotated so that the peak of the fundamental frequency component of the neural response was in the center of the histogram; this usually shifts the peak discharge rate to the center of the histogram. These centered histograms were then averaged across all afferents of each class to obtain measures of the degree to which each afferent type represents the cyclic structure of the gratings.

Vector strength (Goldberg and Brown, 1969) provides an index of the degree of phase locking, which ranges from 0 for uniform discharge at all phases of the stimulus cycle to 1.0 for perfect phase locking (i.e., all spikes occur at one time within the stimulus cycle). Any departure from perfect compactness (all spikes at the same phase) results in a decline in vector strength. Vector strength is computed by representing each action potential by a unit vector with direction determined by its phase within the (centered) cycle histogram, by summing the unit vectors for all action potentials evoked by the stimulus, and by dividing the magnitude of the resultant vector by the magnitude that it would have had if all unit vectors were perfectly aligned to a single phase of the spatial period (i.e., the action potentials were perfectly phase locked). The vector strength expected from firing unrelated to the periodicity of the stimulus was calculated by redistributing the impulses randomly and repeating all of the calculations (including rotation to center the fundamental component). This was repeated 1000 times to get the distribution of vector strengths arising from the null hypothesis (no phase locking to the grating period).

Spatial variation in SA1 firing rates is computed as in our previous studies (Connor et al., 1990; Connor and Johnson, 1992; Blake et al., 1997) with modifications that make it correspond more closely to the physiological properties of neurons in SI cortex. Our computation of spatial variation in firing rates in previous studies was similar to the computation performed by central neurons with excitatory and inhibitory subfields separated by 1–3 mm (Connor and Johnson, 1992). We now know that many neurons in area 3b of the S1 cortex perform just such a computation (DiCarlo and Johnson, 2000), so we use them as a model for computations in the present study. The discharge rates of many neurons in area 3b are proportional (linearly related) to the rectified difference in afferent firing rates between the excitatory (E) and inhibitory (I) subregions of their receptive fields. We perform exactly this computation on the primary afferent responses from two adjacent regions separated by 1–3 mm. The computation is illustrated in Results (see Fig. 8). This computation differs from our previous computations in two ways. First, the summed discharge from each subregion is based on a random sample of afferent responses. This mimics the fact that the excitatory and inhibitory subfields of a neuron are fed by multiple afferents. Second, the integration time t ranges from 5 to 20 msec; that is, the rectified difference in firing rates at any instant is proportional to the difference in the numbers of E and I impulses over the previous time. DiCarlo and Johnson (1999) showed that the integration time for both excitation and inhibition in area 3b neurons is <20 msec (i.e., the SD of the temporal effect is <10 msec).

Spatial variation in SA1 firing rates evoked by each surface was computed with actual SA1 responses (see Fig. 8). SA1 afferents were drawn at random (with replacement) from the experimental sample to simulate the E and I inputs. All of the spikes from the E and I samples were superimposed to make up the summed E and I impulse rates (see Fig. 8). The impulse rate of the (half-wave) rectified difference (E–I) at any instant was based on the number of E and I impulses in the previous t seconds. The measure used for comparison with the psychophysical test was the mean rectified impulse rate over 7 mm of scanning (i.e., 350 msec). Rectification simulates that fact that neurons respond with zero discharge rates when the net drive is inhibitory. This computation was done for many (thousands of) random fiber samples at all possible orientations of the I subfield relative to the E subfield (in increments of 10°) to obtain the mean simulated firing rate for each stimulus surface. This corresponds to the hypothesis that roughness perception is based on the mean firing rate of a population of central neurons that compute the spatial variation in SA1 firing rates. The simulation parameters (numbers of afferents in the E and I subfields, their separation, and the integration time) were varied.

RESULTS

Psychophysical results

Psychophysical data were obtained from 10 subjects (seven males and three females; ages, 22–58 years; median age, 28 years) who reported the roughness of 21 surfaces comprising a smooth surface, 8 triangular gratings with spatial periods ranging from 0.1 to 2.0 mm, and 12 trapezoidal gratings with spatial periods ranging from 0.2 to 2.0 mm (Fig. 1B). The ridge and groove widths are illustrated in Figure 1C. Because the subjects chose their numerical scales arbitrarily, the subjective reports were normalized to a mean value of 1.0 within subjects before averaging across subjects. The mean normalized responses are illustrated in Figure 2. We judged the surfaces to be less rough than those in our previous studies, but the range of roughness judgments (13 to 1) was as large (Connor et al., 1990) or larger (Connor and Johnson, 1992; Blake et al., 1997) than those in any of our previous studies because the smoothest surfaces were less rough.

The psychophysical results are similar to those in previous studies in which gratings were used (Lederman, 1983; Sathian et al., 1989). The roughness judgments were affected primarily by GW (Fig. 2A) and secondarily by RW (Fig. 2B). A regression of the roughness judgments (R) on all of the linear and quadratic terms involving GW (in millimeters) and RW (in millimeters) yielded the following equation:

$$R = 0.2 + 1.6\mathrm{GW} - 0.5\mathrm{RW} - 0.25\mathrm{GW}^2, \quad (1)$$

which accounts for 98% of the variance in roughness judgments. The SD of the residual regression errors (0.08) is only marginally higher than the SEs of the roughness judgment values among the 10 subjects themselves, which averaged 0.06. The *solid lines* in each of the three graphs of Figure 2 represent the roughness judgments predicted by this equation. The negatively accelerating effect of GW^2 is illustrated in Figure 2A. Increasing RW had a negative effect that was independent of GW (Fig. 2B). The effect is generally less than the effect of GW (Eq. 1), but it is not markedly less. The relative contributions of the GW and RW are illustrated by their derivatives; the derivative of roughness (R) with respect to GW declines linearly with increasing GW ($\mathrm{d}R/\mathrm{dGW} = 1.6 - 0.5\mathrm{GW}$), whereas the influence of RW remains

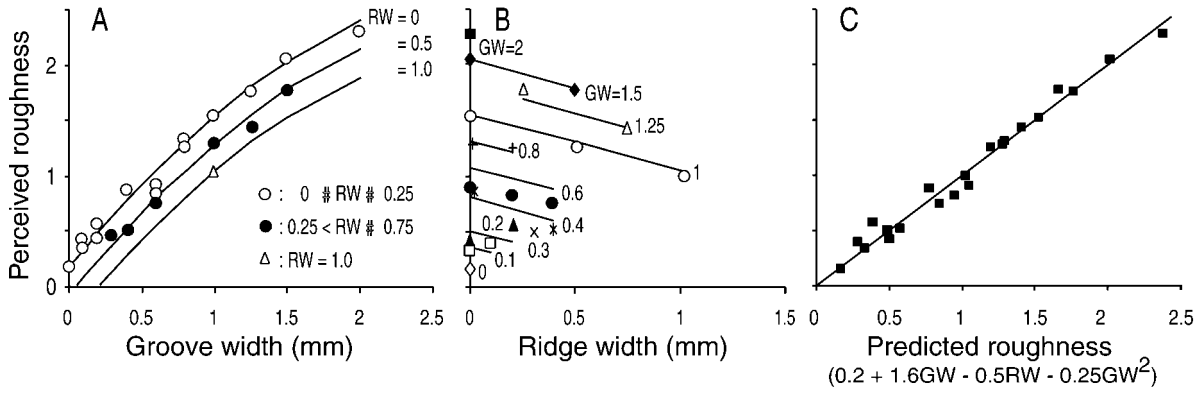

Figure 2. Psychophysical roughness judgments versus groove and ridge width. The *y*-axis in each graph represents the mean normalized roughness judgments from 10 subjects (SEM averaged 0.063; range, 0.013–0.125). The *lines* in each graph represent the values predicted by the following equation: $0.2 + 1.6GW - 0.5RW - 0.25GW^2$. *A*, Roughness judgments are separated into three groups on the basis of RW to show the correspondence with the equation evaluated at three values of RW (0, 0.5, and 1.0 mm). *B*, *Symbols* of a single type represent roughness judgments at single GW values (in millimeters). *C*, The *x*-axis represents the best (least squares) fitting equation involving all linear and second-order terms in GW and RW that are statistically significant.

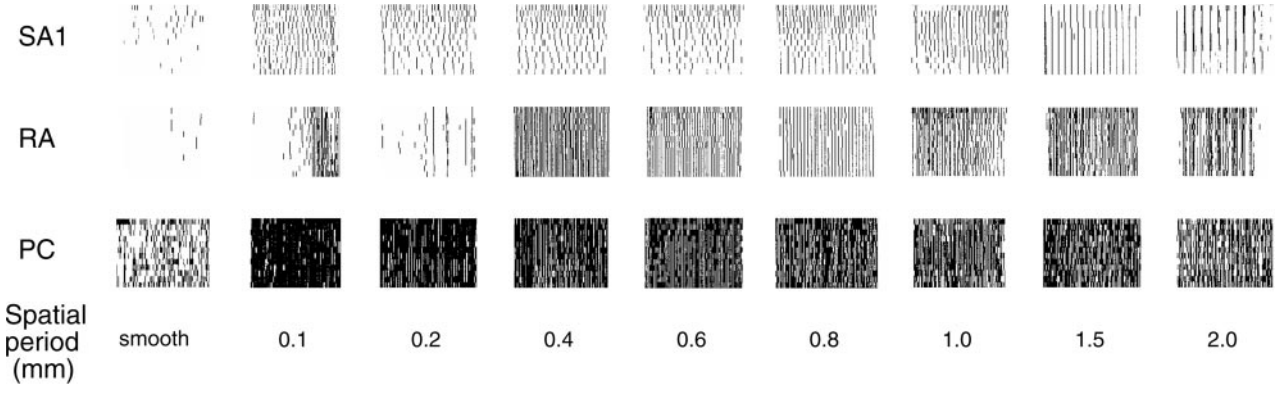

Figure 3. Raster plots of SA1, RA, and PC responses to gratings. Each *tick mark* represents the occurrence of an action potential, and each *horizontal row* of *ticks* represents the response to a single sweep of the stimulus pattern across the receptive field at a velocity of 20 mm/sec. *Successive rows* represent response sweeps of action potentials after consecutive 200 μm shifts of the stimulus perpendicular to the scanning direction. The *rasters* in a *single column* represent responses to a surface with a single spatial period, which is specified at the *bottom*. The grating with the 0.1 mm spatial period is a triangular grating. The rest are trapezoidal gratings with groove widths that are as close to half of the spatial period as the design allows (0.1, 0.2, 0.3, 0.4, 0.6, 1.0, and 1.0 mm groove widths for the 0.2, 0.4, 0.6, 0.8, 1.0, 1.5, and 2.0 mm spatial periods, respectively).

constant at all groove and ridge widths ($dR/dRW = -0.5$). When GW and RW are near zero (fine gratings), GW is approximately three times more important than is RW (cf. Sathian et al., 1989). When GW is greater (coarse gratings), the effects of groove and ridge width are more nearly equal in magnitude, although they work in opposite directions; at GW = 2 mm, for example, $dR/dGW = 0.6$ and $dR/dRW = -0.5$.

Neurophysiological results

Of 34 neurons that were studied (16 SA1, 11 RA, and 7 PC), 22 were studied long enough to provide complete data sets; they comprised nine SA1, seven RA, and six PC afferent fibers. Six SA1 and three RA afferents had receptive fields on the distal fingerpads; the rest had receptive fields on the more proximal phalanges or the palm. There were no apparent differences between the responses of the SA1 and RA afferents on the digital and palmar pads. These data exclude the results from the triangular gratings with periods of >0.1 mm for reasons given in Materials and Methods. The scanning velocity was 20 mm/sec; therefore, the temporal frequency (velocity/spatial period) with which gratings passed over a region of skin ranged from 10 Hz (for the gratings with 2.0 mm spatial periods) to 200 Hz (for the triangular grating with GW = 0.1 mm).

All three afferent types responded to all of the gratings. Several elements of the responses of each type are displayed in Figure 3. The SA1 and RA afferents responded minimally to the smooth surface; the PC impulse rates evoked by the smooth surfaces (mean, 43 impulses/sec) were approximately half of the rates evoked by the gratings (mean, 78 impulses/sec). The SA1 and RA impulse rates are affected by spatial period, but they are more strongly determined by GW and RW (Goodwin et al., 1989). The gratings labeled 0.1 and 0.2 mm have the same GW (0.1 mm), but the RW in the surface with the 0.2 mm spatial period is greater (0.1 vs 0 mm); that is why the afferents respond less vigorously to the grating with the 0.2 mm period illustrated in Figure 3. The PC afferent illustrated in Figure 3 is typical in that its firing rate is largely but not totally unaffected by spatial period; its firing rates match closely with the mean PC firing rates illustrated below (see Fig. 7). Responsiveness to the individual ridges is evident in the firing of all three types. For example, although the SA1 afferent illustrated in Figure 3 is responding to the grating with the 0.1

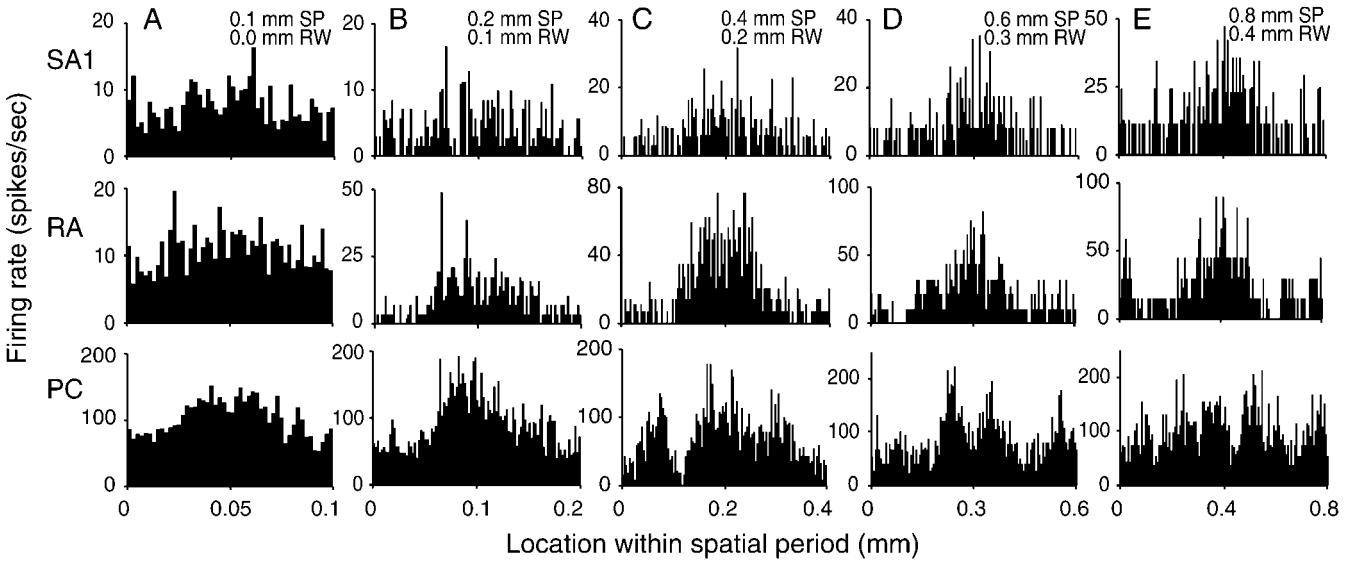

Figure 4. Summed cycle histograms of responses to fine gratings. The spatial period (*SP*) and ridge width of each *column* of histograms (*A–E*) are shown in the *top right corner* of the *top* histogram. Histograms of individual neuronal responses to each grating were rotated to center the peak response and then summed across neurons to produce the histograms displayed here (see Materials and Methods).

mm spatial period with a firing rate of only ~15 impulses/sec (i.e., on approximately every 12th grating cycle), the spike timing is clearly affected by the periodic structure of the grating.

Spatiotemporal response structure

One of the questions motivating the present study was whether SA1 primary afferents would respond to the spatial structure of finely textured surfaces. Cycle histograms of firing in each of the afferent types versus the phase within each grating cycle are shown for five of the finer gratings (Fig. 4). The patterns of modulation illustrated in Figure 4 are those expected from the vibratory sensitivity of each of the three afferent types (Freeman and Johnson, 1982). When gratings with 0.1 mm periods are scanned across the skin at 20 mm/sec, all skin points within the receptive field of a single afferent are stimulated at 200 Hz, albeit at different phases. The resultant stimulus at the transducer site of each receptor is a 200 Hz vibration (plus harmonics). Two hundred Hertz is near the minimum of the PC threshold tuning curve, and consequently, the PCs respond well and are clearly modulated by the stimulus. The response is nearly sinusoidal because the fundamental component is a sinusoid at 200 Hz; the first harmonic at 400 Hz is sufficiently beyond the PC tuning curve so that it has little effect. When the grating period is 0.4 mm (Fig. 4, *column C*), every skin point is stimulated at 50 Hz; the resultant stimulus at each receptor is a complex, periodic stimulus with a fundamental frequency of 50 Hz and, it is presumed, strong harmonic components at 100, 150, 200 Hz, etc. Because 50 Hz is near the minimum of the RA threshold tuning curve and the higher harmonics occur in less sensitive parts of the RA frequency range, the RAs are modulated strongly at the fundamental frequency. Because the maximum SA1 sensitivity occurs at lower frequencies, the SA1s are modulated less strongly by the 0.4 mm grating. The PC cycle histogram is clearly modulated by the 0.4 mm grating period, but the higher harmonics span the region of maximum sensitivity; these higher harmonics are clearly visible in the PC cycle histogram in *column C*. When the grating period is 0.8 mm (Fig. 4, *column E*), the fundamental frequency is 25 Hz. This is near the minimum of the SA1 threshold tuning curve (Freeman and Johnson, 1982), and SA1s are modulated strongly at the fundamental frequency. The RA afferents are modulated nearly equally, but they appear to be responding to the second harmonic (50 Hz) as well. The PCs appear to be responding exclusively to the higher harmonics.

The degree to which each afferent type represented the fundamental grating period was analyzed by computing the vector strength of the response (Goldberg and Brown, 1969). Zero vector strength corresponds to uniform firing rates at all phases of the stimulus cycle; unity vector strength corresponds to perfect entrainment in which spikes only occur at one phase of the cycle. A plot of vector strength versus spatial period (Fig. 5) shows that each afferent type represents the periodic structure of the stimulus most effectively when the stimulus temporal frequency is near its peak temporal sensitivity. Overall, PC afferents represent the stimulus periodicity least strongly because they respond at all phases. The PC modulation is strongest when the grating period is 0.2 mm, which corresponds to a temporal frequency of 100 Hz. The RA vector strength peaks at the 0.4 mm spatial period (50 Hz) as expected from the histograms illustrated in Figure 4. The broad SA1 vector strength shows that the SA1 impulses tend to be more tightly phase locked than are the RA or PC responses at all but the smallest spatial periods. This reflects their greater spatial acuity.

A different view of the temporal structure of the firing patterns that proves more important for roughness coding is illustrated in Figure 6, which shows that all of the responses to these gratings are irregular. Figure 6 shows successive pairs of interspike intervals for all SA1, RA, and PC afferents responding to the 0.2, 0.4, and 0.6 mm spatial periods. If each of the afferents of a single type responded with regular trains of impulses (i.e., successive intervals were equal), the points in the serial interval plots would lie along the 45° diagonal. It is evident that the length of one interspike interval is a poor predictor of the next. In other words, except for a tendency to fire at a specific phase, there is a strong probabilistic component to the discharge. This randomness is the crucial response property that allows spatial variation in the SA1 discharge to account for roughness perception.

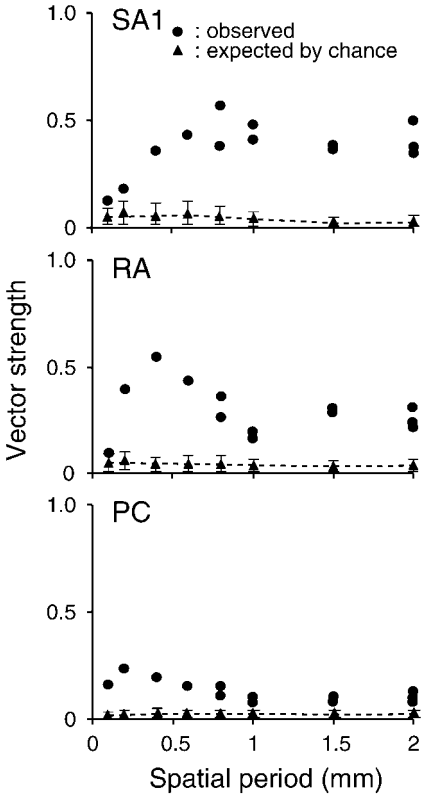

Figure 5. Strength of entrainment to the grating spatial period. Vector strength represents the degree to which impulse firing is entrained by the grating cycles. A value of one corresponds to firing that occurs at only one phase location relative to the passing grating cycles; a value of zero corresponds to uniform firing across all phase locations. Each *filled circle* represents the vector strength of a composite cycle histogram, five of which are displayed for each afferent type in Figure 4. The *filled triangles* represent the vector strengths expected by chance if there was no cyclic entrainment; the error bars represent the 95% confidence intervals (i.e., the region within which vector strength would fall 95% of the time if there was no cyclic entrainment; see Materials and Methods).

Mean impulse rate

The effects of GW, RW, and spatial period on the impulse rates of each of the afferent types are illustrated in Figure 7. The three afferent types differ markedly in their dependence on GW and RW. The plot of impulse rate versus GW (Fig. 7, *top left*) shows that the SA1 discharge rate is determined primarily by GW. When the SA1 impulse rate is plotted against RW (Fig. 7, *middle left*), the data points are more widely scattered. The lines connecting points with a constant spatial period show that RW has a strong negative effect on the firing rate. Regression of SA1 impulse rates on linear and quadratic combinations of GW and RW (Fig. 7, *bottom left*) showed that both parameters affected SA1 impulse rates:

$$\text{SA1 impulse rate} = 1.4 + 30\text{GW} - 11\text{RW}, \qquad (2)$$

in which GW and RW are expressed in millimeters. Only the linear terms were statistically significant. The residual error SD was 2.4 impulses/sec; the regression accounted for 96.4% of the data variance. Notice that GW and RW affected the SA1 firing rates in almost exactly the same proportions (3 to 1) and in the same directions as they affected the roughness judgments (compare with Eq. 1).

The RA impulse rate was equally affected by GW and RW. The linear regression 13 + 34GW − 30RW accounted for 81% of the data variance with a residual SD of 5.8 impulses/sec. No quadratic regression improved the fit. The PC impulse rate was constant and unaffected by both GW and RW. When the regression procedure is forced to include both GW and RW, it yields the formula 79 + 11GW − 31RW, but the regression is not significant ($p = 0.38$). No quadratic regression improved the fit. We include the best fit in Figure 7 for comparison with the SA1 and RA data.

Neural coding

The present study was motivated by two questions. The primary question was whether spatial variation in the SA1 population response could account for roughness perception when the element spacing is <1 mm. A second question, which would have assumed greater importance if the answer to the first question were negative, was whether the PCs might account for roughness perception when the element spacing is fine. Both questions yielded clear answers.

Correlation between the RA mean impulse rate (and spatial or temporal variation in the RA impulse rate) and the subject's roughness judgments was 0.93. We reject hypotheses based on RA codes for two reasons. First, neural codes based on RA responses have been shown to be completely inconsistent with the subjects' roughness magnitude judgments for surfaces coarser than the ones used in this study (Lederman et al., 1982; Johnson and Hsiao, 1994; Blake et al., 1997). Second, SA1 spatial variation accounts well for the perceived roughness of the fine surfaces used in the present study. If a case were made for an RA code, one would have to explain why the nervous system switches to a different neural code (which correlates less well) for fine surfaces.

PC codes

The PC responses were analyzed for mean rate, temporal variation, and spatial variation. The correlation between the PC mean impulse rate and the psychophysical roughness judgments was 0.098, which was not significantly different from zero. Spatial variation was computed with the same algorithm that was used for the SA1 afferents (see below). The result, like the correlation between the mean impulse rate and roughness, was not significantly different from zero. Temporal variation was computed as the difference in firing rates between successive periods as in Connor et al. (1990). The lengths of the integration periods and the time between them were varied from 5 to 50 msec. The correlations with roughness judgments were consistently negative but not significantly different from zero. We could find no signal in the PC response that might come close to accounting for the roughness judgments.

SA1 spatial variation

The hypothesis tested here is that roughness perception depends on a specific neural measure, spatial variation in the SA1 population response. This hypothesis and all of the others considered in this and previous studies from our laboratory are confined to measures of the primary population response that might underlie roughness perception; they do not imply a specific implementation. The question here is the adequacy of the hypothesis that roughness perception depends on the mean absolute (i.e., rectified) difference in firing rates between groups of SA1 afferents with receptive field centers separated by ~2 mm. It is difficult, however, to ignore the fact that this computation is performed by any neuron in the CNS whose receptive field comprises excitatory and inhibitory subfields separated by ~2 mm and the discharge of

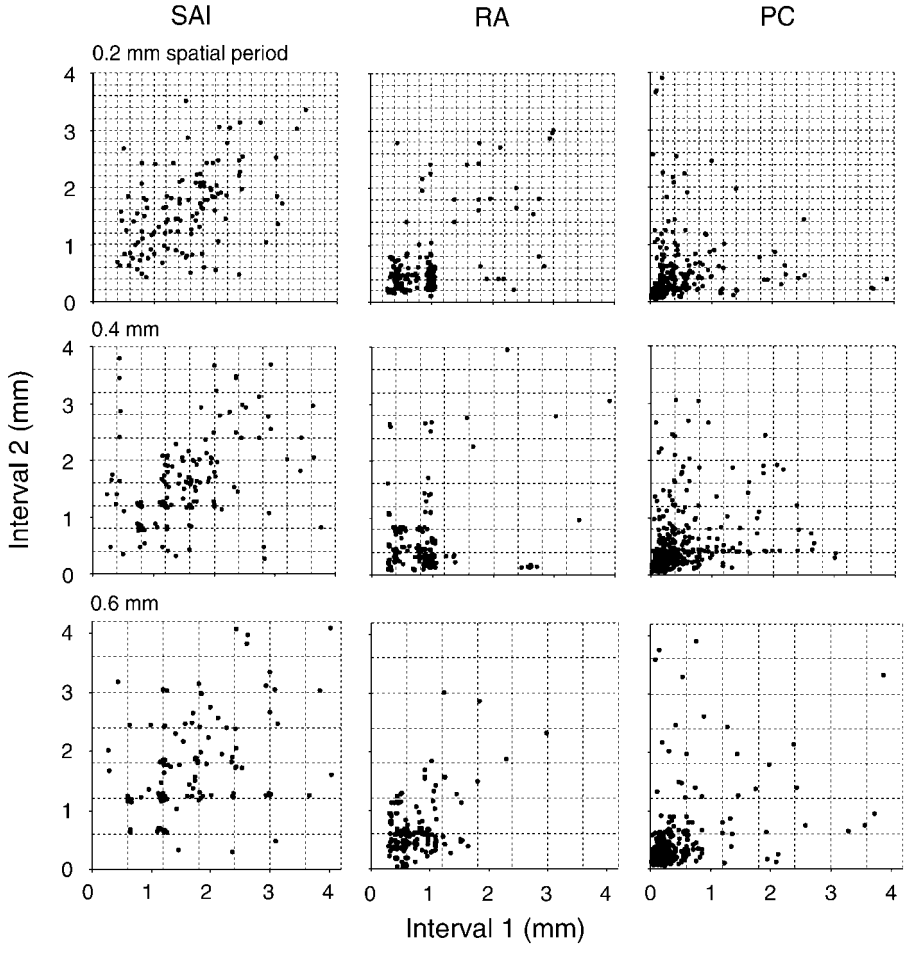

Figure 6. Serial interspike intervals for SA1, RA, and PC responses. Intervals 1 and 2 represent successive intervals within a single sweep. Each plot represents all serial interval pairs evoked by the specified grating for all sweeps and all neurons of the specified type. The units are millimeters. The *grid lines* represent multiples of a single grating cycle. *Points* close to the *grid lines* represent intervals that were close to a multiple of the grating cycle.

which is proportional to the net excitatory drive. Many neurons in area 3b, for example, have these properties (DiCarlo and Johnson, 2000). Therefore, the analysis that follows is also a test of the idea that roughness perception is proportional to the mean firing rate of a population of cortical neurons that compute spatial variation in the SA1 afferent discharge.

Spatial variation in the SA1 discharge is measured as if it was being computed by a neuron with separate *E* and *I* subfields (Fig. 8). The receptive field of the hypothetical neuron is depicted as if viewed through the back of the finger and onto the skin surface contacting the grating. The *E* and *I* parts of the receptive field are each fed by six afferents in the illustration; in the actual calculations the numbers of *E* and *I* afferents ranged from 2 to 20. Displayed to the *left* of the finger are actual SA1 spike rasters from 12 sweeps across one of the gratings (GW, 0.2 mm; RW, 0.2 mm). They are meant to represent a typical afferent drive on the *E* and *I* subfields; it is assumed that the discharge patterns of primary afferents are independent of one another except for the effects of common driving. The summed *E* and *I* drives and their difference, which are illustrated to the *left* of the schematic neuron, fluctuate randomly around their mean rates. The firing rate of this schematic neuron is proportional to the net excitatory drive (DiCarlo et al., 1998).

The correlation between the SA1 spatial variation computed in this way and the subjects' roughness magnitude estimates was almost completely independent of the parameters of the calculation (the numbers of SA1 afferents in the *E* and *I* subfields, the integration time constant, and the distance between the centers of the *E* and *I* subfields); correlation coefficients ranged from 0.961 to 0.992 as the integration time constant ranged from 5 to 20 msec, the *E–I* separation ranged from 1.0 to 3.0 mm, and the numbers of SA1 afferents in the *E* and *I* subfields ranged from 2 to 20 mm^2. The correlation based on parameters matching typical properties of area 3b neurons (integration time, 15 msec; *E–I* separation, 2 mm; 14 SA1 afferents in the *E* and *I* subfields) is illustrated in Figure 9 (0.97 correlation). The basic mechanisms determining spatial variation in the afferent discharge when the element density is higher than the afferent innervation density are examined in the Appendix.

DISCUSSION

The psychophysical results reported here extend the range of spatial periods used in roughness studies to 100 μm; the finest spatial period used previously was 250 μm (Lederman, 1983). Except that we report a slight negative curvature in the relationship between roughness perception and groove width, the results are nearly identical to previous results with gratings (Lederman, 1983; Sathian et al., 1989). The difference may have arisen because we used more and finer surfaces. The equation that fits the data closely ($r^2 = 0.98$) predicts that roughness judgments should reach a maximum at a GW of 3.2 mm and then decline at greater GWs. This matches the results of Connor et al. (1990), who found that when raised-dot patterns (0.35 mm high) are used in roughness magnitude judgment experiments, roughness peaks at a dot spacing of 3.2 mm and declines for greater spacings. This is not a general finding, however; Meftah et al. (2000) report a monotonic

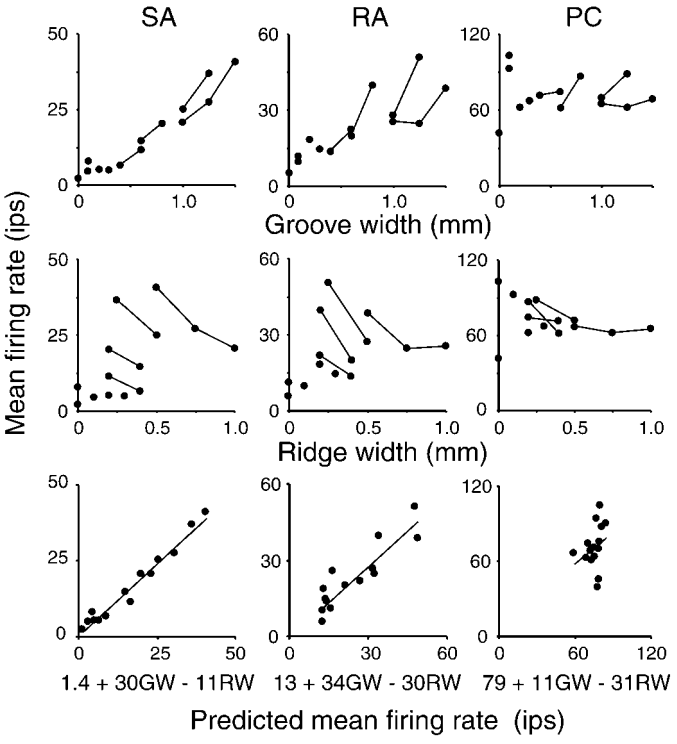

Figure 7. SA1, RA, and PC mean impulse rates versus groove width, ridge width, and the predicted impulse rates. *Solid lines* in the *top two rows* link *points* with the same spatial period. For example, the *three points* linked by a *line* in each of these graphs are impulse rates evoked by gratings with 2 mm spatial periods. The *solid lines* in the *bottom row* are the predicted impulse rates. The r^2 values are 0.97, 0.81, and 0.16 for the SA1, RA, and PC regressions, respectively. The PC regression is not significant. *ips*, Impulses per second.

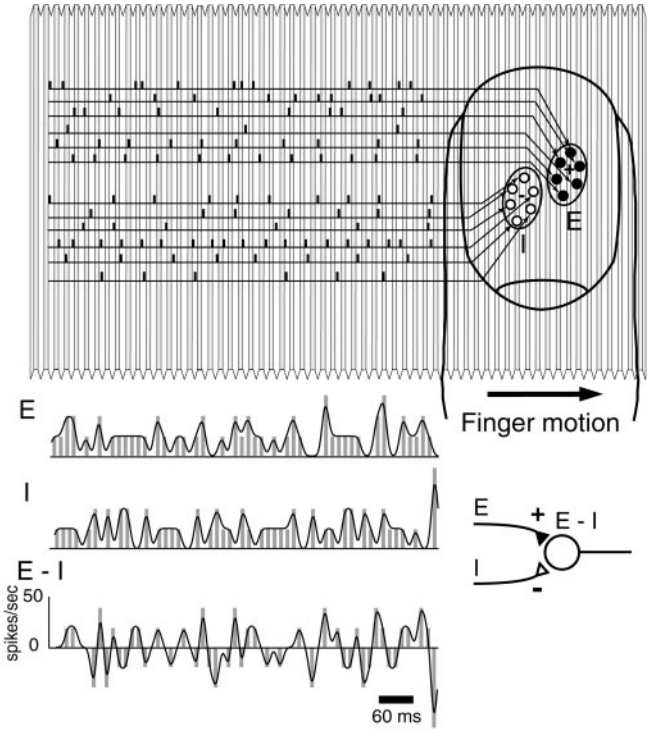

Figure 8. Spatial variation calculations. The model illustrated here corresponds to the calculations used to compute the spatial variation in SA1 firing rates. The hypothesis is that roughness perception is the rectified differences in firing rates between skin regions with centers separated by 1–3 mm. A neuron with *E* and *I* subfields like those illustrated here and with an impulse rate that is proportional to the difference between the *E* and *I* drive at any instant computes the parameter expressed by the spatial variation hypothesis. The diagram illustrates a finger scanning from *left* to *right* across a grating with 0.2 mm groove and ridge widths (0.4 mm spatial period). The finger and grating are not drawn to the same scale. The *E* and *I* regions represent hypothetical excitatory and inhibitory areas, each receiving inputs from six SA1 afferents as an example. The actual number varies from 2 to 20 in the computations. The individual spike trains displayed here were drawn at random from the whole set of responses to the grating with 0.2 mm groove and ridge widths. The *vertical gray bars* in the *rows* marked *E* and *I* represent the summed impulses in 12.5 msec bins in the excitatory and inhibitory afferents, respectively. The *solid line* represents a smoothed (Gaussian kernel, 5 msec SD) estimate of the instantaneous rate. The *row* marked *E–I* plots the difference between *E* and *I* expressed as summed impulse rates. It is meant to represent the net excitatory drive that, when positive, produces a mean firing rate proportional to the difference in firing rates between afferents from the *E* and *I* subfields.

increase in roughness to dot spacings of 8 mm. The difference is probably accounted for by the fact that their dots are much higher (1.8 mm) than are those in any previous study.

The neurophysiological results are difficult to compare with results from previous studies in which gratings were used. The spatial periods used by Darian-Smith and Oke (1980) were predominantly ≤1 mm (540–1025 μm), but they did not vary groove and ridge width and did not report impulse rates; nonetheless it is evident from their study that PC afferents responded most vigorously and SA1 afferents responded least vigorously. Goodwin et al. (1989) and Sathian et al. (1989) varied groove and ridge width, but the grating spatial periods were, with one exception, ≥1 mm; increasing GW had a similar, positive effect on impulse rates in all three afferent types in their studies. In contrast, GW had a significant positive effect on the SA1 and RA responses but had no significant effect on the PC responses in the present study. RW had a minor, almost negligible effect on firing rates in all three afferent types in the studies of Goodwin et al. (1989) and Sathian et al. (1989). In contrast, RW had a strong, negative effect on SA1 and RA responses (Fig. 7) in the present study but no significant effect on the PC responses. The differences are almost certainly explained by differences in spatial periods. For example, the effect of RW in the present study appears to decline when the RW is >0.75 mm (Fig. 7).

Neural coding

We examined two hypotheses. The first was that activity in PC afferents accounts for the perceived roughness of finely textured surfaces. The second was that spatial variation in the impulse rates of SA1 afferents accounts for the perceived roughness of fine surfaces. Both hypotheses assume that SA1 spatial variation accounts for the perceived roughness of coarse surfaces.

The first hypothesis is essentially Katz's duplex hypothesis, advanced by Hollins and his colleagues (Hollins and Risner, 2000; Hollins et al., 2000), that the perceived roughness depends on a spatial mechanism for coarse surfaces and a vibratory mechanism for fine surfaces. Hollins and his colleagues have provided evidence of this hypothesis by showing that intense, high-frequency vibration can make a relatively smooth surface feel less smooth (Hollins et al., 2000). However, after it is demonstrated that the SA1 hypothesis accounts for roughness perception for fine and coarse surfaces, the first hypothesis seems moot. Why (to invoke parsimony) would the nervous system use two different mechanisms when one mechanism accounts for the perceived roughness

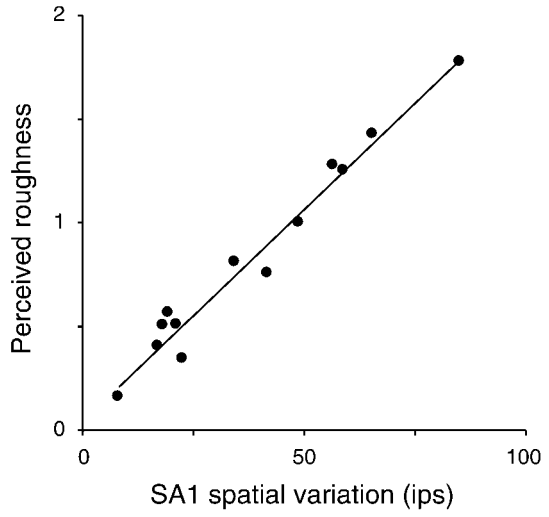

Figure 9. Consistency plot of perceived roughness versus spatial variation of SA1 neural firing rates. Spatial variation was computed with an algorithm that is illustrated in Figure 8 (see Results). Correlation, 0.97.

of both fine and coarse surfaces? But this is a logical, not an empirically based, argument. The empirical finding is that we could, in fact, find no correlation between any measure of the PC discharge and the subjective roughness judgments reported in the psychophysical experiments; because the PCs responded equally vigorously to fine and coarse surfaces (Figs. 3, 7), every PC measure yielded nearly the same predicted roughness. The neural basis for the observations by Hollins and his colleagues is unclear; the intense, high-frequency vibration could have affected the discharge of SA1 and RA afferents as well as that of PC afferents, or it could have affected some central interaction between the PC and SA1 systems (Tommerdahl et al., 1999).

The results support the second hypothesis strongly. One of the puzzles motivating the experiments reported here was the following question: even if the SA1 afferents respond to finely textured surfaces, how can a spatial variation code work when the element density is finer than the SA1 innervation density? The answer is that any stimulus that produces discharge with nonuniform interspike intervals results in fluctuating differences in firing rates between afferents; this, in turn, activates any mechanism sensitive to spatial variation in impulse rates.

SA1 spatial variation accounts for the subjects' reports in subjective magnitude estimation experiments; the question remains whether the same neural code accounts for the subjects' behavior in texture discrimination tasks. The answer depends on whether the subject in the discrimination task is asked to provide an objective or subjective report, the distinction being that an objective report can be scored for accuracy (e.g., right or wrong) and a subjective report cannot. The two tasks are different, and the neural basis for the report is likely to be different (see Craig and Johnson, 2000). If the purpose of the discrimination experiment is to probe a subject's perceptual experience (e.g., that surface A feels rougher than surface B, a subjective response that cannot be scored for accuracy) (Phillips and Matthews, 1993), then we believe that the neural basis for the judgment is the spatial variation in SA1 responses. If, however, the purpose is to determine the subject's ability to discriminate surfaces that differ in element spacing or some other spatial feature (Lamb, 1983; Morley et al., 1983), it is likely that the subject will use whatever neural information is most effective in the particular task. The objective ability to discriminate stimuli and subjective experience have no known relationship (Fechner notwithstanding) (Stevens, 1961); likewise, the neural mechanisms underlying a subject's ability to discriminate stimuli and subjective experience have no obligatory relationship.

Cumulative evidence

The argument that roughness perception is accounted for by variation in firing rates between SA1 afferents is based on the ideas of falsification (Popper, 1959; Platt, 1964); when there are many possible explanations, one can arrive at a single explanation only by demonstrating the adequacy of that explanation and the falseness of the rest. First, consider adequacy. Variation in firing rates between SA1 afferents with receptive field centers separated by ~2 mm has now accounted for roughness judgments in four studies with 62 surfaces that varied in surface geometry, element spacings that varied from 100 μm to 6.2 mm, heights that varied from 280 μm to 2.0 mm, and widths that varied from 0 mm (triangular gratings) to 2.5 mm. The correlation between psychophysical roughness magnitude estimates and spatial variation in the SA1 discharge was >0.97 in every study; the correspondence is illustrated in Figure 10. There are no data of which we are aware that suggest that SA1 spatial variation does not account for roughness perception. Second, consider falseness. The test of the falseness of a putative neural code in these studies was inconsistency, not just that it fitted the results less well than did another hypothesis. If two surfaces evoke neural responses with the same neural coding measure (e.g., PC impulse rate) but one is perceived as smooth and the other rough, then that measure cannot be the basis for the two percepts. The consistency test has resulted in the rejection of all codes based on PC responses (Lederman et al., 1982; Connor et al., 1990; and the present study), all codes based on RA responses (Lederman et al., 1982; Johnson and Hsiao, 1994; Blake et al., 1997), all codes based on SA2 responses [by analysis of data reported in Phillips et al. (1992) and Phillips and Matthews (1993)], all codes based on mean impulse rate (Connor et al., 1990; Connor and Johnson, 1992), and all temporal codes (Connor and Johnson, 1992).

Our working hypothesis is that the brain uses a single neural coding mechanism for all surfaces. An alternative possibility is that different neural codes are used for different surfaces. It could be argued, for example, that SA1 mean impulse rate cannot be rejected for fine gratings because it correlates with roughness perception (0.97) as well as does SA1 spatial variation (0.97). But, as argued previously, why would the brain switch codes from a neural mechanism that applies universally (SA1 spatial variation) to one that is frequently unrelated to roughness? The SA1 mean impulse rate is anticorrelated with roughness perception for some surfaces, positively correlated for some, and uncorrelated for others (Johnson and Hsiao, 1994). However, we show in the Appendix that SA1 spatial variation depends on SA1 mean impulse rate when the surface features are too fine to be resolved by SA1 afferents. Therefore, there is an indirect relationship between roughness perception and SA1 mean rate for finely textured surfaces.

Neural mechanisms

The rejection of all putative neural coding measures except spatial variation in the SA1 impulse rate does not involve any assumptions about neural mechanisms. All hypotheses were phrased in terms of putative neural measures, and all conclusions were of the type "roughness cannot depend on x (e.g., PC rate)

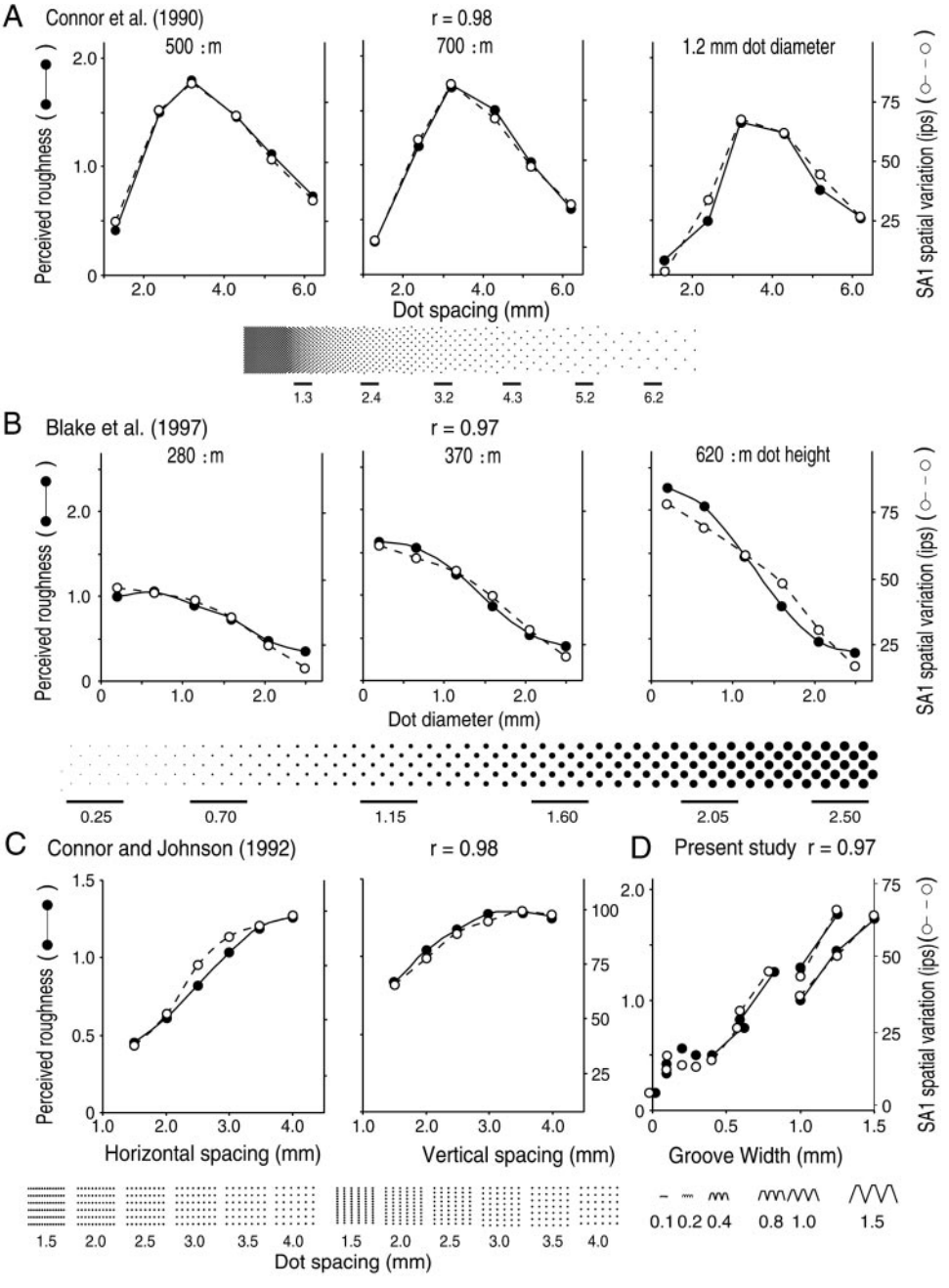

Figure 10. Perceived roughness and measures of spatial variation in firing rates in four studies with different textured surfaces. The *left y*-axis in each graph is the mean reported roughness. The *right y*-axis is the spatial variation in SA1 firing rates. The surface pattern used in each study is illustrated below the data to which the pattern applies. The impulse rates from the first three studies have been rescaled to be approximately consistent with the rates in the present study. *A*, Results from Connor et al. (1990) who used 18 raised-dot patterns with different mean dot spacings and diameters. The pattern segment corresponding to each dot spacing is shown below the data. *B*, Results from Blake et al. (1997) who used 18 raised-dot patterns with different dot heights and diameters. The pattern segment corresponding to each mean dot diameter is shown below the data. *C*, Results from Connor and Johnson (1992) who varied pattern geometry to distinguish temporal and spatial neural coding mechanisms. *D*, Data from the present study. The *solid lines* connect stimulus patterns with constant spatial periods as in Figure 7.

because surfaces that vary widely in perceived roughness evoke responses with the same value of *x*." Therefore, our hypothesis that roughness perception depends on spatial variation in SA1 impulse rates does not imply any specific neural implementation. Nonetheless, spatial variation in afferent impulse rates is computed by every central neuron with excitatory and inhibitory subfields.

A mechanistic hypothesis that we favor is that roughness perception is based on the mean firing rate of a subpopulation of neurons in area 3b (or area 1) with excitatory and inhibitory subfields separated by ~2 mm and with response properties like those described by DiCarlo and Johnson (2000). To test this hypothesis, we have done psychophysical experiments in which subjects scan different surfaces with two adjacent fingers and are asked to attend to just one finger. If roughness is computed by neurons with receptive fields spanning several fingers (e.g., in S2 cortex), then roughness judgments at the attended finger should be affected by the roughness of the adjacent surface, but they are not (Dorsch et al., 2001).

Conclusion

First, and most important, we conclude that the same neural mechanism accounts for the perceived roughness of both fine and coarse surfaces. This mechanism measures the difference in firing rates between SA1 afferent fibers with receptive field centers separated by 2–3 mm. This difference can result from spatial variation in the stimulus pattern on a scale of 2–3 mm, from stochastic fluctuation between afferents with receptive fields separated by 2–3 mm, or from a combination of these two sources of spatial variation. Second, this mechanism corresponds closely to known mechanisms within the central somatosensory pathways. Our favored working hypothesis is that SA1 spatial variation is

computed by cortical neurons with receptive fields comprising excitatory and inhibitory subfields separated by 2–3 mm and that roughness perception depends on the mean firing rate of this cortical subpopulation. Where this might happen is not known. Specific hypotheses about cortical mechanisms need to be subjected to the same consistency test that we have used in this and previous studies.

APPENDIX: Determinants of SA1 spatial variation

The model neuron illustrated in Figure 8 implements the computations that we believe underlie roughness perception. Our hypothesis is that roughness perception depends on the mean firing rate of a population of neurons with receptive fields like that illustrated in Figure 8. Whether that is the actual mechanism underlying roughness perception or not, the model provides a vehicle for examining the spatial variation computation closely. The parameters (integration time constant and excitatory and inhibitory field sizes) of the model neuron are based on typical properties of neurons in area 3b of SI cortex (DiCarlo and Johnson, 2000).

The instantaneous firing rate of the model neuron is proportional to the difference d between the inputs to the E and I subfields over an integration period of ~15 msec. That difference has two components, a deterministic component that is dependent on the stimulus surface structure and a stochastic component. When the stimulus pattern is dominated by feature elements spaced at >1–2 mm from one another, the difference is dominated by spatial variation in the SA1 firing rates caused by the spatial structure of the stimulus. For example, when a finger is scanned over an array of raised dots separated by a millimeter or more, the SA1 neural population response is an isomorphic neural image of the stimulus pattern (Connor et al., 1990; Phillips et al., 1992), and the difference d is determined primarily by the dot spacing and secondarily, if at all, by intrinsic fluctuation in the firing. When the elements composing the stimulus pattern are too dense to be resolved by the SA1 afferent population response, as they are for most surfaces in this study, the variation in firing rates between afferent fibers is dominated by stochastic fluctuations in the firing rates of the individual fibers.

The computation E–I illustrated in Figure 8 is a spatial derivative. Because derivatives, spatial or temporal, amplify stochastic variation, the difference mechanism is driven strongly by stochastic fluctuation in the SA1 population response to a finely textured surface. Below we show, using Poisson statistics, that the fluctuation in SA1 firing rates is proportional to the square root of the mean SA1 firing rate. Therefore, the perceived roughness of a finely textured surface is determined by the degree to which it activates SA1 afferents.

The mean firing rate of the model neuron is proportional to the average value of the positive part of d (i.e., the mean, half-wave rectified value of E–I) (see Fig. 8). This is half the first absolute moment of the distribution of d when E and I are balanced. To calculate this absolute moment, we make several assumptions. We assume (1) that the afferent fiber responses contributing to E and I are independent of one another, (2) that their superposition approximates a Poisson process, (3) that E and I are balanced, and (4) that d is normally distributed with a zero mean. The first assumption has no experimental justification of which we are aware, but it is widely assumed to be true. The second assumption is justified whether or not the individual spike trains are Poisson. A spike train composed of independent, superimposed spike trains tends toward a Poisson process as the number of contributing spike trains increases (Cox and Lewis, 1966). When the spike timing in the individual input fibers is already random, as illustrated in Figure 6, the convergence is rapid. We comment on the third assumption at the end of the Appendix. The fourth assumption is justified by the central limit theorem; i.e., the E–I difference is the summed effect of the action potentials in a dozen or more independent afferent fibers.

To be specific, d is taken to be the difference in impulse counts activating the E and I subregions within a 15 msec integration period. When d is normally distributed or nearly normal, the mean value of the positive part of d is proportional to the SD of d (the proportionality constant being the square root of $1/2\pi$). Computer simulations using SA1 responses show that this proportionality is exact to within 10% when individual SA1 impulse rates are at least 4 impulses/sec (with 14 SA1 afferents converging on E and I and an integration period of 15 msec). The variance of d (i.e., SD squared) is the sum of the variances of the E and I impulse counts (because the individual afferent responses are assumed to be independent). Because the contributions of E and I are assumed to be Poisson, the variance of the 15 msec impulse count difference equals the mean sum of the counts in the E and I subregions. That sum is proportional to the SA1 mean rate. Therefore, when E and I are balanced, the mean firing rate of the model neuron is proportional to the square root of the mean SA1 firing rate. The correlation between roughness perception and SA1 spatial variation is ~0.97 because the correlation with the square root of the SA1 mean firing rate is ~0.97.

This analysis is based on the assumption that E and I are balanced [and, in fact, many neurons in the SI cortex have balanced excitation and inhibition (DiCarlo et al., 1998)], but that assumption is not necessary. The excitatory mass in area 3b, for example, is ~25% greater on average than the inhibitory mass (DiCarlo et al., 1998). In that case, the net drive on the neuron is excitatory, and the mean suprathreshold drive is some combination of the mean afferent rate and its SD. Therefore, the conclusion is not critically dependent on the assumption that E and I are exactly balanced. The correlation would have been 0.97 even if we had assumed that the drive was entirely excitatory.

Note that this analysis applies only when the deterministic part of the SA1 population response is essentially uniform (i.e., finely textured surfaces). In the transition from fine to coarse structure, spatial variation in the SA1 population response depends in part on stochastic fluctuation and in part on spatial variation in the deterministic part of the response.

REFERENCES

Blake DT, Hsiao SS, Johnson KO (1997) Neural coding mechanisms in tactile pattern recognition: the relative contributions of slowly and rapidly adapting mechanoreceptors to perceived roughness. J Neurosci 17:7480–7489.

Connor CE, Johnson KO (1992) Neural coding of tactile texture: comparisons of spatial and temporal mechanisms for roughness perception. J Neurosci 12:3414–3426.

Connor CE, Hsiao SS, Phillips JR, Johnson KO (1990) Tactile roughness: neural codes that account for psychophysical magnitude estimates. J Neurosci 10:3823–3836.

Cox DR, Lewis PAW (1966) The statistical analysis of series of events. London: Methuen.

Craig JC, Johnson KO (2000) The two-point threshold: not a measure of tactile spatial resolution. Curr Dir Psychol Sci 9:29–32.

Darian-Smith I, Kenins P (1980) Innervation density of mechanoreceptive fibers supplying glabrous skin of the monkey's index finger. J Physiol (Lond) 309:147–155.

Darian-Smith I, Oke LE (1980) Peripheral neural representation of the spatial frequency of a grating moving across the monkey's finger pad. J Physiol (Lond) 309:117–133.

DiCarlo JJ, Johnson KO (1999) Velocity invariance of receptive field

structure in somatosensory cortical area 3b of the alert monkey. J Neurosci 19:401–419.
DiCarlo JJ, Johnson KO (2000) Spatial and temporal structure of receptive fields in primate somatosensory area 3b: effects of stimulus scanning direction and orientation. J Neurosci 20:495–510.
DiCarlo JJ, Johnson KO, Hsiao SS (1998) Structure of receptive fields in area 3b of primary somatosensory cortex in the alert monkey. J Neurosci 18:2626–2645.
Dorsch AK, Hsiao SS, Johnson KO, Yoshioka T (2001) Tactile attention: subjective magnitude estimates of roughness using one or two fingers. Soc Neurosci Abstr 27:50.2.
Freeman AW, Johnson KO (1982) A model accounting for effects of vibratory amplitude on responses of cutaneous mechanoreceptors in macaque monkey. J Physiol (Lond) 323:43–64.
Goldberg JM, Brown PB (1969) Response of biaural neurons of dog superior olivary complex to dichotic tonal stimuli: some physiological mechanisms of sound localization. J Neurophysiol 32:613–636.
Goodwin AW, John KT, Sathian K, Darian-Smith I (1989) Spatial and temporal factors determining afferent fiber responses to a grating moving sinusoidally over the monkey's fingerpad. J Neurosci 9:1280–1293.
Hollins M, Risner SR (2000) Evidence for the duplex theory of tactile texture perception. Percept Psychophys 62:695–705.
Hollins M, Fox A, Bishop C (2000) Imposed vibration influences perceived tactile smoothness. Perception 29:1455–1465.
Johansson RS, Vallbo ÅB (1979) Tactile sensibility in the human hand: relative and absolute densities of four types of mechanoreceptive units in glabrous skin. J Physiol (Lond) 286:283–300.
Johnson KO, Hsiao SS (1994) Evaluation of the relative roles of slowly and rapidly adapting afferent fibers in roughness perception. Can J Physiol Pharmacol 72:488–497.
Johnson KO, Phillips JR (1988) A rotating drum stimulator for scanning embossed patterns and textures across the skin. J Neurosci Methods 22:221–231.
Katz D (1925) The world of touch. Reprint (Krueger LE, translator). Hillsdale, NJ: Erlbaum, 1989.
Lamb GD (1983) Tactile discrimination of textured surfaces: psychophysical performance measurements in humans. J Physiol (Lond) 338:551–565.
Lederman SJ (1974) Tactile roughness of grooved surfaces: the touching process and the effects of macro- and microsurface structure. Percept Psychophys 16:385–395.
Lederman SJ (1983) Tactual roughness perception: spatial and temporal determinants. Can J Psychol 37:498–511.
Lederman SJ, Loomis JM, Williams DA (1982) The role of vibration in the tactual perception of roughness. Percept Psychophys 32:109–116.
Meftah EM, Belingard L, Chapman CE (2000) Relative effects of the spatial and temporal characteristics of scanned surfaces on human perception of tactile roughness using passive touch. Exp Brain Res 132:351–361.
Morley JW, Goodwin AW, Darian-Smith I (1983) Tactile discrimination of gratings. Exp Brain Res 49:291–299.
Mountcastle VB, LaMotte RH, Carli G (1972) Detection thresholds for stimuli in humans and monkeys: comparison with threshold events in mechanoreceptive afferent nerve fibers innervating the monkey hand. J Neurophysiol 35:122–136.
Phillips JR, Matthews PBC (1993) Texture perception and afferent coding distorted by cooling the human ulnar nerve. J Neurosci 13:2332–2341.
Phillips JR, Johansson RS, Johnson KO (1992) Responses of human mechanoreceptive afferents to embossed dot arrays scanned across fingerpad skin. J Neurosci 12:827–839.
Platt JR (1964) Strong inference. Science 146:347–353.
Popper K (1959) The logic of scientific discovery. New York: Basic Books.
Sathian K, Goodwin AW, John KT, Darian-Smith I (1989) Perceived roughness of a grating: correlation with responses of mechanoreceptive afferents innervating the monkey's fingerpad. J Neurosci 9:1273–1279.
Stevens SS (1961) To honor Fechner and repeal his law. Science 133:80–86.
Talbot WH, Darian-Smith I, Kornhuber HH, Mountcastle VB (1968) The sense of flutter-vibration: comparison of the human capacity with response patterns of mechanoreceptive afferents from the monkey hand. J Neurophysiol 31:301–334.
Tommerdahl M, Delemos KA, Whitsel BL, Favorov OV, Metz CB (1999) Response of anterior parietal cortex to cutaneous flutter versus vibration. J Neurophysiol 82:16–33.
Vega-Bermudez F, Johnson KO (1999) Surround suppression in the responses of primate SA1 and RA mechanoreceptive afferents mapped with a probe array. J Neurophysiol 81:2711–2719.